Mechanical Technology and Engineering Insights

www.mtei.reapress.com

Mech. Technol. Eng. Insights . Vol. 2, No. 2 (2025) 68–81.

Paper Type: Original Article

Nonlinear Low-Velocity Impact Analysis of a Rectangular Composite Plate Reinforced with Shape Memory Alloy Strips Based on Local and Instantaneous Phase Transformations

Rita De Fátima Muniz[1,*], Ramin Goudarzi Karim[2]

[1] Programa de Pós-graduação em Educação Núcleo de Avaliação Educacional, Federal University of Ceará, 60430-160 Fortaleza, Brazil; ritafatimamuniz@gmail.com.

[2] Department of CIS, Stillman College, Tuscaloosa, Alabama, USA; rkarim@stillman.edu.

Citation:

Received: 12 November 2024 *Revised: 01 Februray 2025* *Accepted: 14 April 2025*	De Fátima Muniz, R., & Goudarzi Karim, R. (2025). Nonlinear low-velocity impact analysis of a rectangular composite plate reinforced with shape memory alloy strips based on local and instantaneous phase transformations. *Mechanical Technology and Engineering Insights, 2*(2), 68-81.

Abstract

In this paper, a nonlinear low-velocity impact analysis of a rectangular composite plate reinforced with Shape Memory Alloy (SMA) strips is conducted, and the effect of the impactor's energy on the impact response of the plate is investigated. In this research, in order to extract accurate results that can be utilized for the validation of future theoretical findings, the instantaneous changes and spatial non-uniformity of the austenite-to-martensite phase transformation (and vice versa) have been considered for the first time. Furthermore, instead of utilizing approximate plate theories, three-dimensional simulation has been employed to extract impact responses based on the theory of three-dimensional elasticity, the implicit result of which is the modification of the contact law. The analysis results demonstrate that the SMA, by forming a hysteresis loop during the impact, leads to a reduction in the energy absorbed by the composite plate; the result of this is an increase in the impact resistance of the composite plate and a reduction in the resulting damage. Moreover, the results indicate that by increasing the impactor's energy, the martensite fraction, contact force, and the deflection at the point of impact increase. The contact duration increases when the impact energy is increased by increasing the impactor's mass; however, it decreases when the impact energy is increased by increasing the impactor's velocity.

Keywords: Low-velocity impact, Composite plate, Shape memory alloy, Local and instantaneous phase transformations.

1 | Introduction

Composite structures, despite their increasing application in various industries, are vulnerable to impact loads. This deficiency can be improved by incorporating shape memory wires or strips into these structures. Shape Memory Alloys (SMAs) are a specific group of smart materials that can absorb or dissipate mechanical energy under cyclic mechanical loading through the creation of a reversible hysteresis loop. This unique characteristic

Corresponding Author: ritafatimamuniz@gmail.comc.ir

https://doi.org/10.48313/mtei.v2i2.39

of SMAs has rendered them suitable for applications in sensing, actuation, impact energy absorption, and vibration damping.

One of the most significant failure mechanisms in composite structures under low-velocity impact is interlaminar separation or delamination, which often stems from the resin's weakness in withstanding interlaminar shear stresses. The presence of SMAs, due to their high energy absorption capacity through phase transformation, can act as a barrier against the propagation of matrix cracks and delamination. Recent studies have shown that the variable stiffness of these alloys during dynamic loading can modify the stress distribution in the impact zone and reduce stress concentration, which is the primary factor in damage initiation [1]. Additionally, the bridging effect provided by embedded wires or strips increases the ultimate resistance of the structure against impactor penetration [2].

Qidwai and Lagoudas [1] proposed a three-dimensional thermomechanical model to predict the damage of thin SMA layers embedded in composite structures using plane stress assumptions. Kim et al. [4] numerically investigated the effect of embedded SMA thin films in composite plates on improving the damage resistance of composite structures under low-velocity impact. Paine and Rogers [5] studied the damage resistance of SMA composites under low-velocity and high-velocity impact. Wu et al. [6] investigated the superelastic effect of SMAs in improving the low-velocity impact resistance of a single-layer composite plate using the finite element method. In this research, the Newmark numerical integration method was used to solve the dynamic finite element equation, and the Hertz contact law was utilized. Several other researchers [7], [8] also investigated the impact behavior of hybrid composite plates with SMAs using numerical solution methods. They quite simply considered only a constant recovery stress for the SMA, which is insufficient for investigating the effect of the SMA on the impact behavior. Jia [9] investigated the impact resistance of SMA hybrid composite structures. He presented a theoretical model to establish a relationship between the martensite fraction, applied load, and the strain energy absorbed in the SMA. Turner et al. [10] attempted to manufacture and test hybrid composites containing SMAs.

In research conducted to date, the modeling of SMA behavior has not been appropriately performed, as the martensite volume fraction (a critical factor in determining the properties of the SMA and its recovery force) has been assumed to be constant. In this paper, for the first time in SMA simulation, the effects of instantaneous changes and the spatial non-uniformity of the austenite-to-martensite phase transformation (and vice versa) have been taken into account. Furthermore, instead of employing approximate plate theories, three-dimensional simulation has been used to extract impact responses based on the theory of three-dimensional elasticity, the implicit result of which is the modification of the contact law. Finally, the effect of the impactor's energy on the impact response of the plate has been investigated.

2 | Low-Velocity Impact Analysis of the Composite Plate

To validate the results, the experimental low-velocity impact test results of a sandwich plate with composite skins are compared with the results obtained from the three-dimensional impact simulation in ABAQUS software. The sandwich plate under consideration is a panel with dimensions of 76.2×76.2 mm2. Each composite skin consists of six layers with a thickness of 0.264 mm. The composite skins are made of carbon/epoxy, the mechanical properties of which are listed in *Table 1*. The core consists of a foam layer with a thickness of 12.7 mm, whose properties are provided in *Table 2*. This assembly is formed with the layup configuration [02/902/02/core/02/902/02]. The boundary conditions of the sandwich plate are of the simply supported type. The impactor is a rigid spherical body with a diameter of 25.4 mm and a mass of 1.8 kg, which strikes the sandwich plate at a velocity of 3.7 m/s (equivalent to an energy of 12.32 J).

The use of three-dimensional elasticity theory, as opposed to classical and first-order shear deformation plate theories, offers a significant advantage in the accurate prediction of transverse stresses.

$\sigma zz, T_{xz}, T_{yz}$

In impact problems, due to the concentration of the load in a small area, a severe stress gradient is created through the thickness, which two-dimensional theories are unable to model correctly. Given that the initiation of damage in hybrid composites is often influenced by these out-of-plane stresses, three-dimensional modeling substantially increases the reliability of the results, particularly in predicting the separation between the SMA and the polymer matrix [11].

Table 1. Mechanical properties of the sandwich plate skin materials.

Material	Carbon/Epoxy	Glass/Epoxy
E_{11} (GPa)	54	32.062
E_{22} (GPa)	54	10.789
E_{33} (GPa)	4.84	10.789
G_{12} (GPa)	3.16	11.92
G_{13} (GPa)	1.87	11.92
G_{23} (GPa)	1.87	4.68
V_{12}	0.06	0.344
V_{13}	0.313	0.344
V_{23}	0.313	0.344
p (kg/m³)	1511	1796

Table 2. Mechanical properties of the foam core.

Property	Value
E (GPa)	0.18
V	0.286
p (kg/m³)	110

The comparison of the results of the present analysis with the experimental results of reference [12] in *Fig. 1* confirms the accuracy of the present analysis method. Following the validation of the present analysis results, the core was removed from the sandwich plate, and the two upper and lower skins were integrated together; additionally, the material of the composite skins was changed from the carbon/epoxy to the glass/epoxy specified in *Table 1*. The geometric model of the composite plate is shown in *Fig. 2*, and the analysis results are presented in *Fig. 3*.

As is evident from the results, by removing the core and changing the material of the composite skins from carbon/epoxy to glass/epoxy, the contact force, the deflection at the point of impact, and the contact duration have increased, while the energy absorbed by the structure during the impact has decreased. The values for peak contact force, impact point deflection, contact duration, and absorbed energy have been extracted from *Fig. 3* for the composite plate and are presented in *Table 3*.

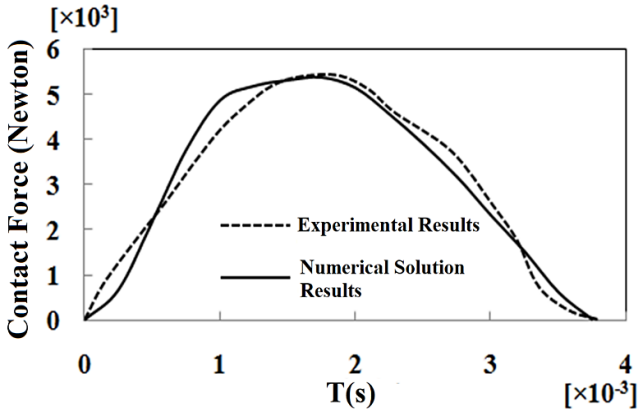

Fig. 1. Validation plot of the present analysis results against the experimental results of reference [12].

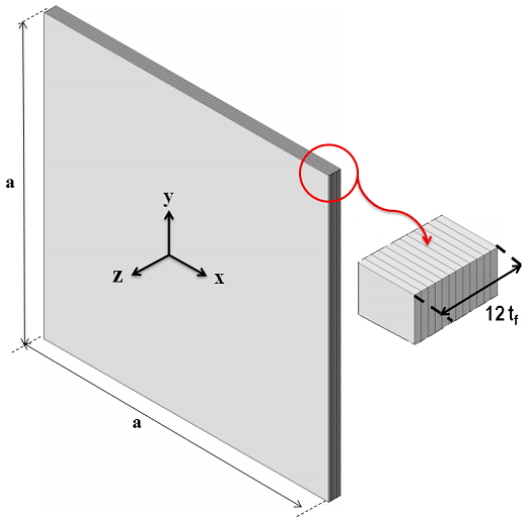

Fig. 2. Geometric model of the composite plate.

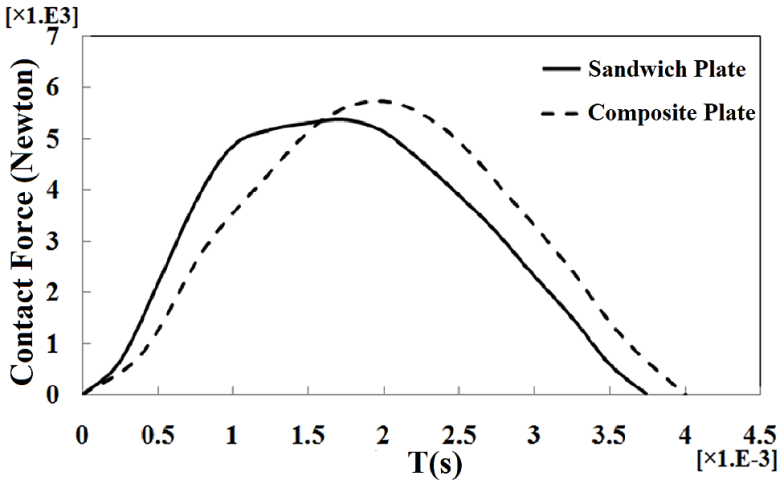

a.

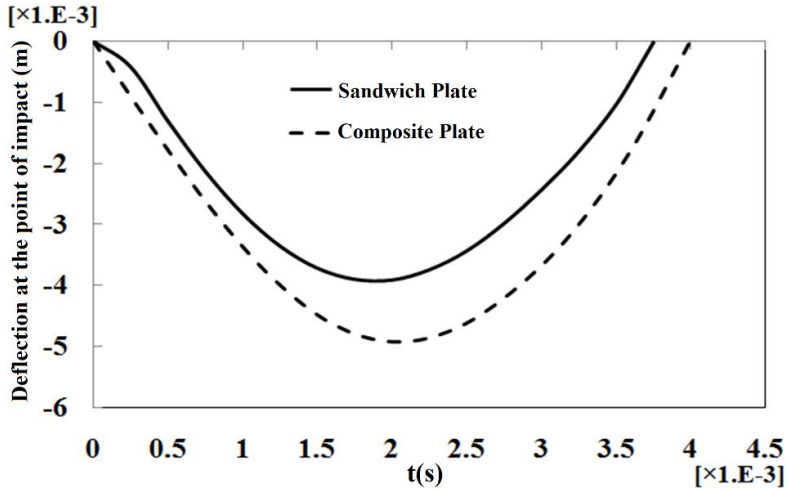

b.

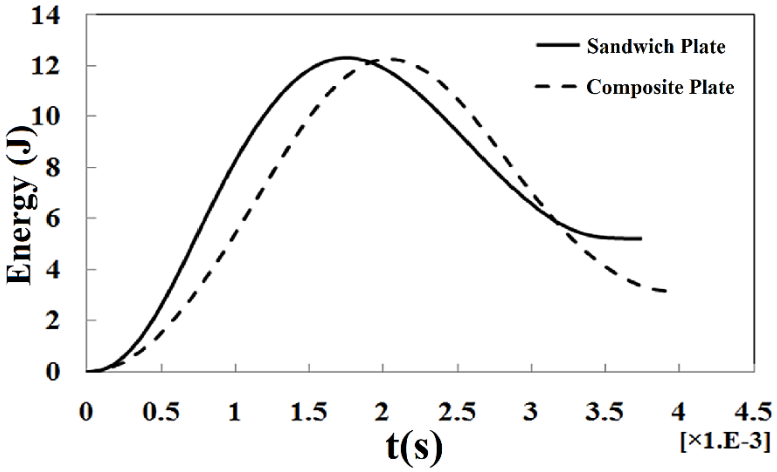

c.

Fig. 3. Time history plots; a. contact force, b. deflection at the impact point, and c. absorbed energy.

Table 3. Values of various parameters in the low-velocity impact response of the composite plate.

Peak Contact Force (kN)	Deflection at Impact Point (mm)	Absorbed Energy (J)	Contact Duration (ms)
5.720	4.91	3.147	4

3 | Effect of Shape Memory Alloy Strips

SMAs possess more than one type of crystal structure or phase. In these alloys, the stable phase at high temperatures and low stress is called austenite, while the stable phase at low temperatures and high stress is called martensite. These two phases are transformable into one another through the application of temperature or stress. This very transformation process affects all mechanical, electrical, and thermal properties of SMAs and establishes them as smart materials. If the SMA is in the austenite phase, applying stress to this material results in the transformation of austenite into detwinned martensite. Upon unloading, the martensite phase becomes unstable, and the reverse transformation occurs; as a result of this transformation, the material returns to its initial state, and no residual strain remains. This behavior is termed superelasticity (or pseudoelasticity) (*Fig. 4*) [13].

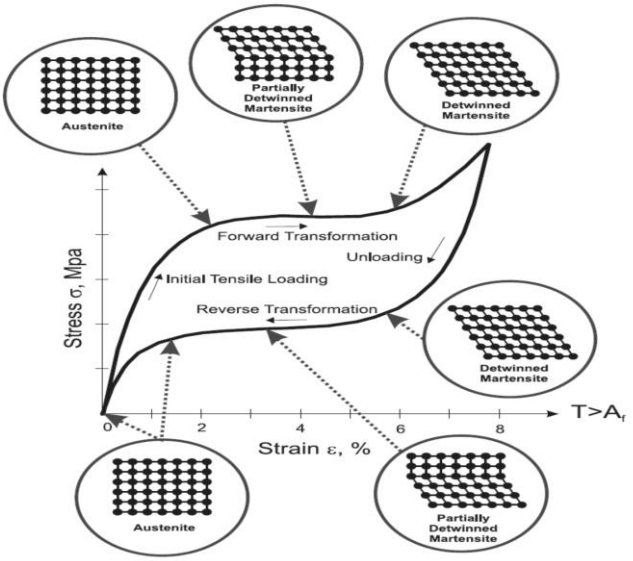

Fig. 4. Stress-strain curve of SMA with superelastic property [13].

In this paper, the effect of the superelastic property and energy-damping characteristics of SMAs on the low-velocity impact response of SMA-reinforced composite plates is investigated. To model the superelastic behavior of the SMA, the Auricchio and Taylor model [14] is utilized. This model is based on the concept of generalized plasticity and is consistent with physical principles. In this model, strain is divided into two components: a fully linear elastic component (ε^{el}) and a component related to martensitic transformation (ε^{tr}):

$$\Delta\varepsilon = \Delta\varepsilon^{el} + \Delta\varepsilon^{tr} \quad (1)$$

The transformation from austenite to martensite occurs via shear forces when these forces reach a specific stress level, which is a characteristic of the material.

$$\Delta\varepsilon^{tr} = a\Delta\zeta\frac{\partial F}{\partial\sigma} \quad (2)$$

$$F^{S} \leq F \leq F^{F}$$

In *Eq. (2)*, ζ is the martensite fraction, and F is the martensitic transformation potential function. The same relationship holds for the reverse martensitic transformation; however, at different stress levels, the intensity of the martensitic transformation follows the stress potential law:

$$\Delta\zeta = f(\sigma,\zeta)\Delta F \quad (3)$$

Any change in the direction of stress results in a reorientation of the martensite. Temperature changes cause a shift in the stress levels at which martensitic transformation takes place. Due to the volume increase during this transformation, less stress is required in tension compared to compression. This phenomenon is modeled using the linear Drucker-Prager criterion for the martensitic transformation potential:

$$F = \bar{\sigma} - p\tan\beta + CT, \quad (4)$$

where $\bar{\sigma}$ is the Mises equivalent stress, p is the compressive stress, and T is the temperature. The rule of mixtures is used to examine the linear elasticity changes from the austenite phase to the martensite phase. The constitutive model presented by Auricchio and Taylor, by considering the temperature dependence of critical transformation stresses, follows the Clausius-Clapeyron relationship. This feature allows the model to account for the effect of latent heat released or absorbed during phase change (although in low-velocity impact, the process is usually assumed to be adiabatic) within the stress variations. The parameter C in *Eq. (4)* exactly

represents the slope of the stress-temperature curve in the alloy's phase diagram, which controls the material's sensitivity to temperature changes during dynamic loading [15].

The input data for the code written to model the superelastic property of SMAs are shown in *Fig. 5*. The properties of the Nitinol materials used in this paper were obtained from uniaxial tensile test results under loading, unloading, and reverse loading conditions, as well as temperature effects (*Table 4*) [16].

Table 4. Properties of nitinol material.

Parameter	Symbol	Value
Austenite Young's modulus	E_A (MPa)	51,700
Austenite Poisson's ratio	ν_A	0.3
Martensite Young's modulus	E_M (MPa)	47,800
Martensite Poisson's ratio	ν_M	0.3
Martensitic transformation strain	ϵ_L	0.063
Stress-temperature variation rate (loading)	C_M [MPaT^{-1}]	6.527
Critical stress for the start of transformation (loading)	σ_S^{AS} (MPa)	600
Critical stress for the end of transformation (loading)	σ_F^{AS} (MPa)	670
Reference temperature	T_0 (°C)	37
Stress-temperature variation rate (unloading)	C_M [MPaT^{-1}]	6.527
Critical stress for the start of transformation (unloading)	σ_S^{AS} (MPa)	288
Critical stress for the end of transformation (unloading)	σ_F^{AS} (MPa)	254
Critical transformation stress in compression	σ_C (MPa)	900

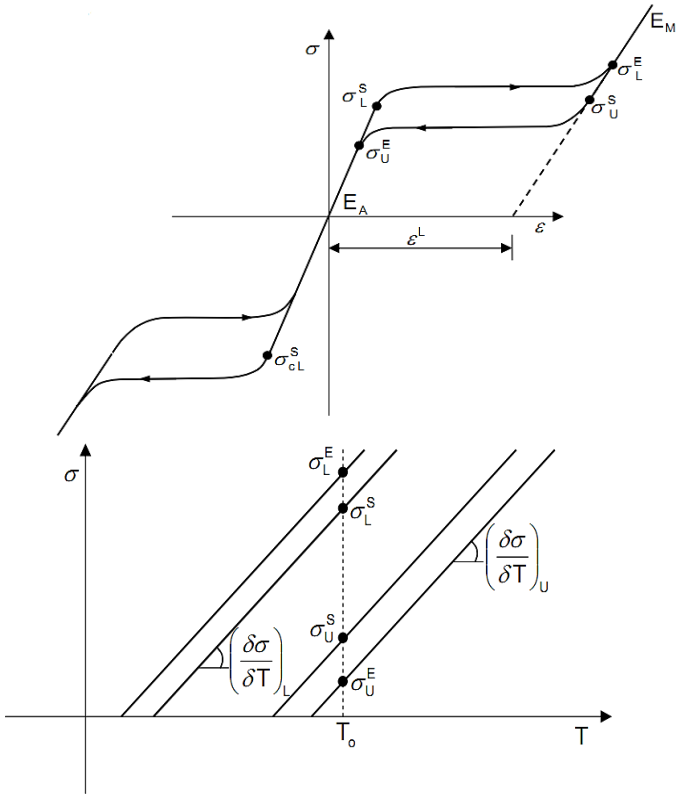

Fig. 5. Input data for simulating the superelastic property of SMAs.

To investigate the effect of the presence of SMAs on the impact response of the composite plate, strips of this alloy were embedded in the first and second layers of the composite plate. The cross-sectional width of these strips is 8 mm, and their thickness was selected to be equal to the thickness of the composite layers (0.264 mm). The length of these strips is equal to the length of the composite plate (76.2 mm) (*Fig. 6*). The analysis results are presented in *Fig. 7*. *Table 5* provides the percentage changes of various parameters compared to the initial state of the composite plate without SMAs. As observed, by embedding strips of SMA

in the composite plate, given that this alloy possesses higher stiffness than the composite plate and that these alloy strips are embedded exactly at the impact location, this factor leads to an increase in the apparent stiffness of the contact zone, the result of which is an increase in the contact force and a decrease in the deflection at the point of impact. On the other hand, SMAs, due to their superelastic property and the formation of a hysteresis loop, possess a high energy absorption capacity. Consequently, by absorbing energy during the impact, this alloy reduces the energy absorbed by the composite plate, which results in an increase in the impact resistance of the composite plate and a reduction in the damage caused by the impact.

In fact, the energy absorption mechanism by SMAs is based on "energy dissipation due to internal friction" during the movement of phase boundaries and twins. The energy reduction absorbed by the composite plate (the matrix section and glass/carbon reinforcing fibers), which is evident in *Table 5*, directly implies a reduction in the energy available for the creation of matrix cracks and interlaminar separation. In other words, the SMA strips play the role of an "energy fuse" that, by sacrificing energy within their hysteresis cycle, prevents destructive energy from reaching the brittle and fragile sections of the composite [17].

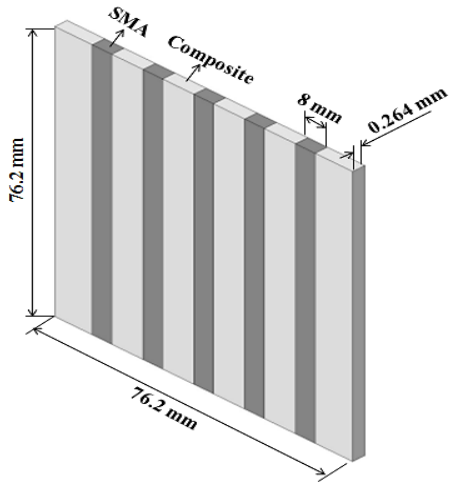

Fig. 6. Embedding of SMA strips within a composite layer.

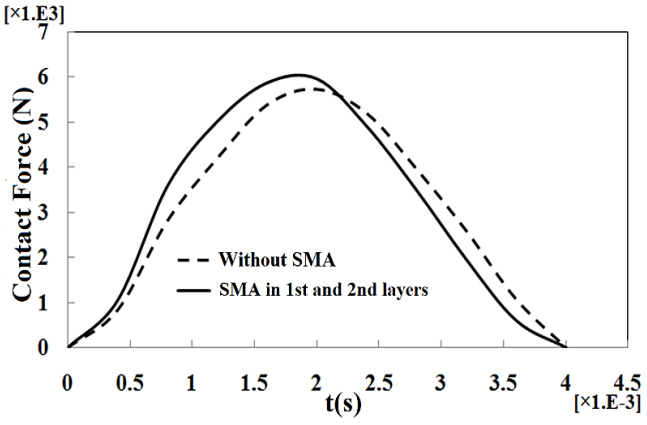

a.

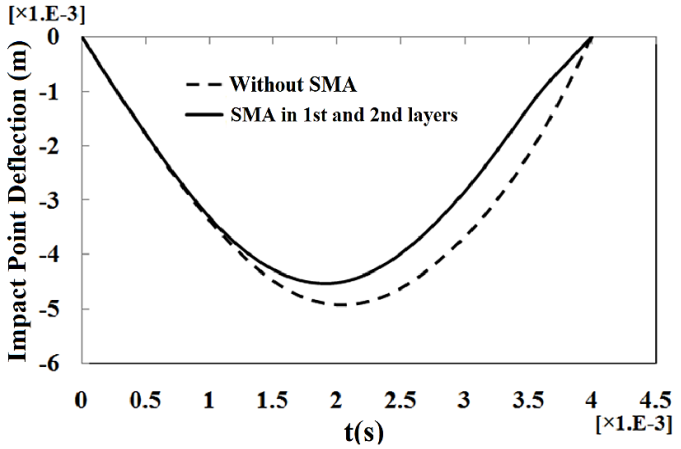

b.

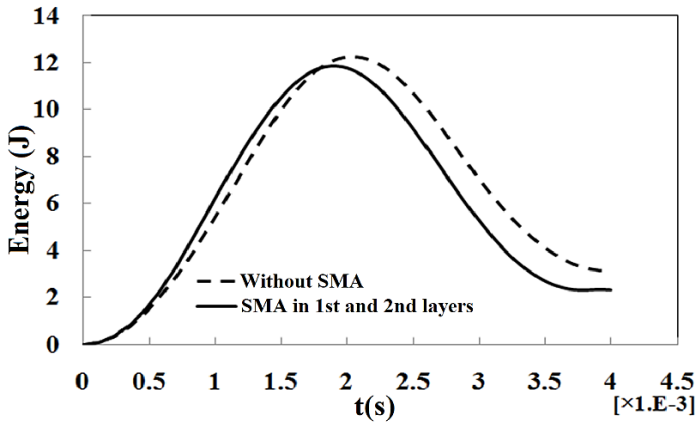

c.

Fig. 7. Effect of the SMA on the time history of: a. contact force, b. deflection at the impact point, c. energy absorbed by the composite plate.

Table 5. Percentage changes in various response parameters for the case with SMA compared to the initial state (absence of SMA).

23.4%	Percentage increase in contact force
14.8%	Percentage decrease in impact point deflection
26.05%	Percentage decrease in absorbed energy

As previously stated, in the present research, the effects of instantaneous changes and the spatial non-uniformity of the austenite-to-martensite phase transformation (and vice versa) have been considered for the first time. For the SMA elements at the impact location (the elements identified in *Fig. 8*), the variations in the martensite volume fraction are shown in *Fig. 9*. As observed, in the element at the impact point, which experiences the maximum deflection and the largest stress values, all of the initial austenite is transformed into martensite. However, as the distance from the impact point increases, the martensite volume fraction decreases due to the reduction in the stress field. Consequently, in element 11, the stress does not reach the critical threshold for the austenite-to-martensite transformation; thus, no portion of the initial austenite is converted to martensite.

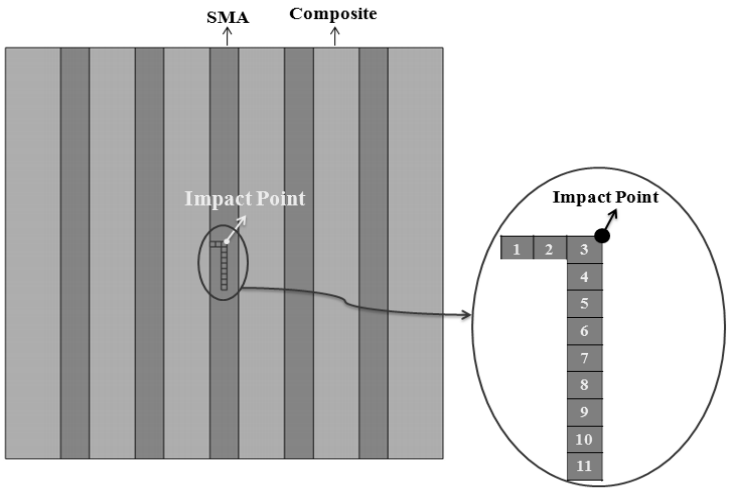

Fig. 8. SMA elements at the impact location and its surrounding area.

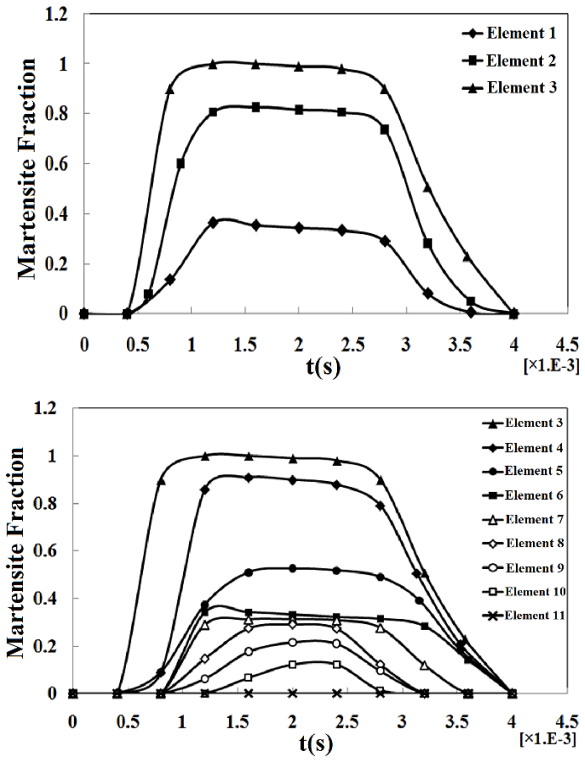

Fig. 9. Martensite volume fraction of the SMA elements at various elements within and around the impact zone.

4 | Effect of Impactor Energy

To investigate the effect of impactor energy on the impact response of the SMA-reinforced composite plate, the impact energy was increased from 12.32 J by factors of 4, 9, and 16. For this purpose, two different methods were employed: first, while keeping the impactor mass constant at 1.8 kg, the impactor velocity was increased from 3.7 m/s by factors of 2, 3, and 4. Second, while keeping the impactor velocity constant at 3.7 m/s, the impactor mass was increased from 1.8 kg by factors of 4, 9, and 16. This approach allows for comparing the differences between these two methods of increasing impact energy in addition to studying the effect of the energy itself on the structural response. The analysis results are shown in *Fig. 10* and *Fig. 11*.

As the impactor energy increases, the martensite volume fraction of the SMA elements increases. For example, as observed in *Fig. 10*, by increasing the impact energy from 12.32 J to 197.13 J, the martensite volume fraction of Element 11 increased from zero to one.

The maximum values for contact force, deflection at the point of impact, and contact duration were extracted from *Fig. 11* for various impactor energy levels and are presented in *Table 6*. *Table 7* provides the percentage changes of these parameters compared to the initial state (impactor with a velocity of 3.7 m/s and a mass of 1.8 kg, equivalent to an energy of 12.32 J).

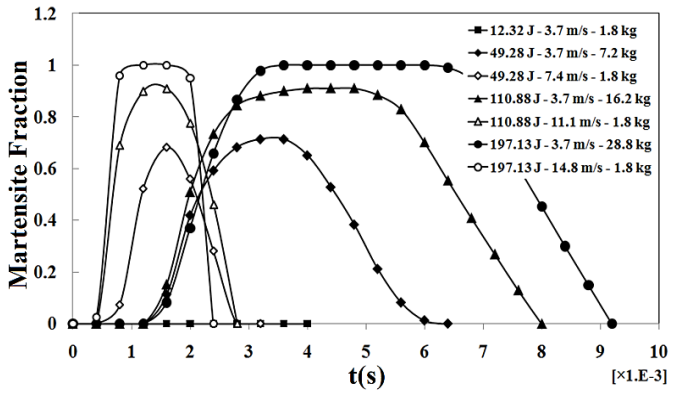

Fig. 10. Martensite volume fraction of Element 11 for various impactor energy levels.

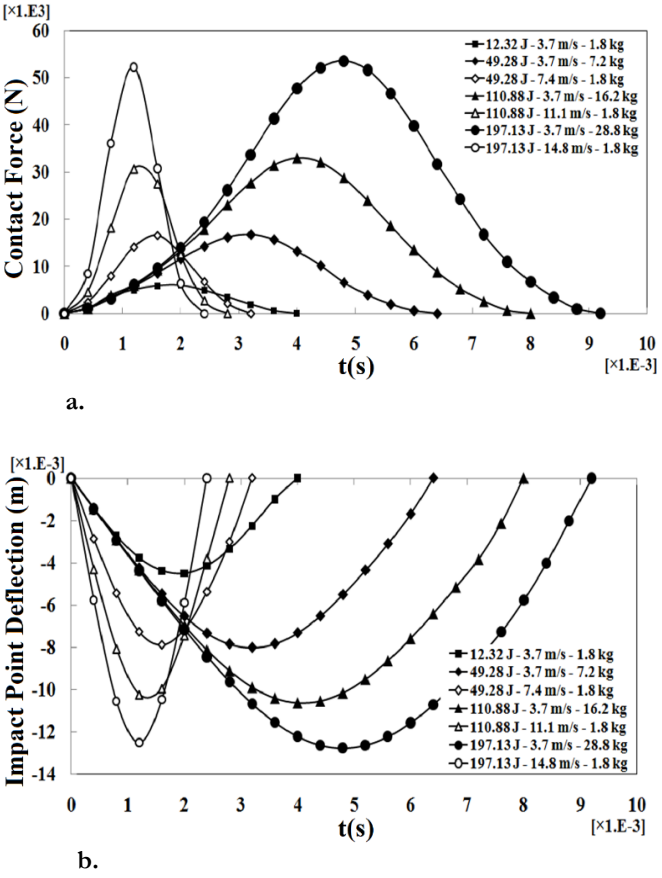

Fig. 11. Effect of impactor energy on the time history of: a. contact force, b. deflection at the impact point.

Table 6. Values of various parameters at different impactor energy levels.

Impact Energy (J)	Impactor Velocity (m/s)	Impactor Mass (kg)	Maximum Contact Force (kN)	Impact Point Deflection (mm)	Contact Duration (ms)
12.32	3.7	1.8	5.962	4.51	4
49.28	7.4	1.8	16.581	7.89	3.2
49.28	3.7	7.2	16.808	8.01	6.4
110.88	11.1	1.8	30.702	10.23	2.8
110.88	3.7	16.2	32.989	10.64	8
197.13	14.8	1.8	52.295	12.50	2.4
197.13	3.7	28.8	53.577	12.77	9.2

Table 7. Percentage changes in various parameters due to the increase in impactor energy compared to the initial impactor state with an energy of 12.32 J.

Impact Energy (J)	Impactor Velocity (m/s)	Impactor Mass (kg)	Percentage Increase in Contact Force (%)	Percentage Increase in Impact Point Deflection (%)	Percentage Change in Contact Duration (%)
49.28	7.4	1.8	178.11	74.94	-20
49.28	3.7	7.2	181.90	77.61	60
110.88	11.1	1.8	414.96	126.83	-30
110.88	3.7	16.2	453.32	135.92	100
197.13	14.8	1.8	777.14	177.16	-40
197.13	3.7	28.8	798.64	183.15	130

As observed from *Fig. 11*, *Table 6,* and *Table* 7, increasing the impactor energy leads to an increase in both the contact force and the deflection at the point of impact. Interestingly, the contact duration increases when the impact energy is raised by increasing the impactor mass; however, it decreases when the impact energy is raised by increasing the impactor velocity.

The difference in contact time behavior stems from the difference in the dynamic response of the structure to "momentum" and "energy." In the case where energy increases through an increase in velocity, wave phenomena and local deformations (such as indentation) become dominant, giving the structure less time for a global and flexural response; thus, the contact duration decreases. However, when the mass increases, the inertia of the impactor forces the entire structure into low-order flexural vibration modes. Consequently, the process of transferring the kinetic energy of the impactor into the strain energy of the structure occurs over a longer time interval. This behavior is consistent with the theory of large-mass impact on plates (quasi-static response) described by Olsson [18].

5 | Conclusion

In this paper, a nonlinear analysis of low-velocity impact on a rectangular composite plate reinforced with SMA strips was conducted. To extract accurate results with minimal error, the instantaneous changes and the spatial and temporal non-uniformity of the austenite-to-martensite phase transformation (and vice versa) were considered for the first time in SMA modeling using VUMAT coding within the Abaqus software. Furthermore, rather than relying on approximate plate theories, a three-dimensional simulation based on elasticity theory was utilized to extract impact responses, which implicitly results in the refinement of the contact law. The most significant findings of this research are as follows:

Energy absorption and damage reduction: the superelastic property of the SMA allows it to absorb a significant amount of energy during impact by forming a hysteresis loop. This absorption reduces the energy taken up by the composite plate itself, leading to increased impact resistance and a reduction in the resulting damage.

Impact energy dynamics: increasing the impactor energy leads to an increase in both the contact force and the deflection at the point of impact. Specifically, the contact duration increases when the impact energy is

raised by increasing the impactor mass, whereas it decreases when the energy is raised by increasing the impactor velocity.

Conflict of Interest

The authors declare that there is no conflict of interest regarding the publication of this article.

Data Availability

All data generated or analyzed during this study are included in this published article. No additional data are available.

Funding

This research did not receive any specific grant from funding agencies in the public, commercial, or not-for-profit sectors.

References

[1] Meo, M., Marulo, F., Guida, M., & Russo, S. (2013). Shape memory alloy hybrid composites for improved impact properties for aeronautical applications. *Composite structures*, *95*, 756–766. https://doi.org/10.1016/j.compstruct.2012.08.011

[2] Cantwell, W. J., & Morton, J. (1991). The impact resistance of composite materials—a review. *Composites*, *22*(5), 347–362. https://doi.org/10.1016/0010-4361(91)90549-V

[3] Qidwai, M. A., & Lagoudas, D. C. (2000). Numerical implementation of a shape memory alloy thermomechanical constitutive model using return mapping algorithms. *International journal for numerical methods in engineering*, *47*(6), 1123–1168. https://doi.org/10.1002/(SICI)1097-0207(20000228)47:6%3C1123::AID-NME817%3E3.0.CO;2-N

[4] Kim, E. H., Lee, I., Roh, J. H., Bae, J. S., Choi, I. H., & Koo, K. N. (2011). Effects of shape memory alloys on low-velocity impact characteristics of composite plate. *Composite structures*, *93*(11), 2903–2909. https://doi.org/10.1016/j.compstruct.2011.05.013

[5] Paine, J. S. N., & Rogers, C. A. (1995). Shape memory alloys for damage-resistant composite structures. *Active materials and smart structures* (Vol. 2427, pp. 358–371). SPIE. https://doi.org/10.1023/A:1004692329247

[6] Wu, Y., Wu, Y., Wang, Y., & Zhong, W. (2007). Study on the response to low-velocity impact of a composite plate improved by shape memory alloy. *Acta mechanica solida sinica*, *20*(4), 357–362. https://doi.org/10.1007/s10338-007-0742-9

[7] Birman, V., Chandrashekhara, K., & Sain, S. (1996). An approach to optimization of shape memory alloy hybrid composite plates subjected to low-velocity impact. *Composites part b: Engineering*, *27*(5), 439–446. https://doi.org/10.1016/1359-8368(96)00010-8

[8] Khalili, S. M. R., Shokuhfar, A., Malekzadeh, K., & Ghasemi, F. A. (2007). Low-velocity impact response of active thin-walled hybrid composite structures embedded with SMA wires. *Thin-walled structures*, *45*(9), 799–808. https://doi.org/10.1016/j.tws.2007.01.017

[9] Jia, H. (1998). Impact damage resistance of shape memory alloy hybrid composite structures. https://vtechworks.lib.vt.edu/items/944fe2c7-849f-47e8-8e22-176b367ac977

[10] Turner, T. L., Lach, C. L., & Cano, R. J. (2001). Fabrication and characterization of sma hybrid composites. *Smart structures and materials 2001: active materials: Behavior and mechanics* (Vol. 4333, pp. 343–354). SPIE. https://doi.org/10.1117/12.432774

[11] Reddy, J. N. (2003). *Mechanics of laminated composite plates and shells: Theory and analysis*. CRC press. https://doi.org/10.1201/b12409

[12] Anderson, T. A. (2005). An investigation of SDOF models for large mass impact on sandwich composites. *Composites part b: engineering*, *36*(2), 135–142. https://doi.org/10.1016/j.compositesb.2004.05.002

[13] Lagoudas, D. s. (2008). *Shape memory alloys : Modeling and engineering applications*. https://searchworks.stanford.edu/view/9106713

[14] Auricchio, F., Taylor, R. L., & Lubliner, J. (1997). Shape-memory alloys: Macromodelling and numerical simulations of the superelastic behavior. *Computer methods in applied mechanics and engineering*, *146*(3–4), 281–312. https://doi.org/10.1016/S0045-7825(96)01232-7

[15] Hartl, D. J., & Lagoudas, D. C. (2009). Constitutive modeling and structural analysis considering simultaneous phase transformation and plastic yield in shape memory alloys. *Smart materials and structures*, *18*(10), 104017. https://doi.org/10.1088/0964-1726/18/10/104017

[16] Kleinstreuer, C., Li, Z., Basciano, C. A., Seelecke, S., & Farber, M. A. (2008). Computational mechanics of Nitinol stent grafts. *Journal of biomechanics*, *41*(11), 2370–2378. https://doi.org/10.1016/j.jbiomech.2008.05.032

[17] Saeedi, A., & Shokrieh, M. M. (2017). Effect of shape memory alloy wires on the enhancement of fracture behavior of epoxy polymer. *Polymer testing*, *64*, 221–228. https://doi.org/10.1016/j.polymertesting.2017.10.009

[18] Olsson, R. (2000). Mass criterion for wave controlled impact response of composite plates. *Composites part a: Applied science and manufacturing*, *31*(8), 879–887. https://doi.org/10.1016/S1359-835X(00)00020-8